JOURNAL OF PROPULSION AND POWER
Vol. 22, No. 5, September–October 2006

Axisymmetric Inlet Design for Combined-Cycle Engines

Jesse R. Colville,* Ryan P. Starkey,† and Mark J. Lewis‡
University of Maryland, College Park, Maryland 20742-3015

Performance considerations for a turbine-based combined-cycle engine inlet are presented using the inlet of the Lockheed SR-71 as a baseline. The methodology incorporated is to modify the SR-71 inlet to expand its operational envelope to higher speeds. A numerical model is developed using the axisymmetric method of characteristics to perform full inviscid flow analysis, including any internal shock reflections. Starting characteristics are quantified based on the Kantrowitz limit. The original SR-71 inlet is analyzed throughout the designed flight regime, beginning at Mach 1.7 and ending with the shock-on-lip condition at Mach 3.2. A series of modifications are then considered for their ability to extend the range of the inlet into the hypersonic flight regime. The results show that two modifications, the widened shoulder centerbody and the variable cone with reextension, have the ability to remain started into the Mach 6–7 range and have similar compressive performance to each other across the entire Mach spectrum.

Nomenclature

A	=	area
M	=	Mach number
m	=	mass flow
P	=	pressure
r	=	radial location
T	=	temperature
x	=	axial location
γ	=	ratio of specific heats
χ	=	flowfield property

Subscripts

av	=	average quantity
max	=	maximum quantity
min	=	minimum quantity
t	=	total (stagnation) quantity
0	=	freestream quantity
2	=	entrance to cowl
4	=	inlet throat

I. Introduction

THE development of turbine-based combined-cycle (TBCC) engines could pave the way for future single-stage-to-orbit and/or two-stage-to-orbit reusable launch vehicles and high-speed missiles. TBCC systems are designed to merge the low-speed attributes of turbojets with the high-speed capabilities of ramjets and scramjets. The integration of the TBCC cycle modes into a single system poses a considerable challenge; each requires unique flow properties to operate properly. Of particular importance is that the inlet must provide efficient compression for all three components across a wide Mach spectrum. Recent TBCC cycle analysis[1] has demonstrated that inlet performance imposes a significant constraint on the overall operation of the engine and can be, in fact, the limiting factor for maximum operational performance.

The criteria for designing both supersonic and hypersonic inlets have been well documented in the literature.[2–4] Some key issues are as follows: 1) diffusing the required amount of air needed for engine performance while minimizing shockwave and viscous loss and maximizing total pressure recovery, 2) supplying the air with tolerable flow distortion, 3) minimizing the amount of added external drag to the vehicle, 4) minimizing added mass to the vehicle, 5) providing a self-starting capability at the required Mach number.

Fernandez et al.[5] discuss some of the major design issues specifically concerning combined-cycle inlets and outline a roadmap for an advanced inlet program to develop the critical inlet technologies. The particular topics the authors focused on in the study are the transition from one cycle mode to another, boundary-layer control, distortion, unstart, and overall performance. Their analysis, conducted with one-, two-, and three-dimensional computational models, showed that the distortion, performance degradation, and total pressure recovery issues need to be addressed before any practical design is realized.

Another design concern for TBCC inlets is identifying a specific design speed. Inlets for a cruising vehicle are traditionally designed at the cruise speed because a large amount of time is spent flying at that velocity. On the other hand, an inlet for an accelerating aircraft (such as the first stage of a two-stage-to-orbit vehicle) must transition through a wide range of velocities, and so choosing a single or even multiple discrete design points for the inlet poses a tougher task.

This study examines a new strategy for designing inlets for TBCC engines. Instead of designing a completely new inlet, the approach will be to build on the knowledge of existing supersonic inlets used on previous TBCC-like engines. The process will examine the effects of overspeeding a known inlet and then incorporate design changes using variable geometry in an attempt to increase its operational range into the hypersonic flight regime. To this end, the limit of previous high-speed inlet designs will be explored, to both determine their maximum speeds and identify means of extending their operational velocities.

For this present work, the benchmark for a TBCC-like engine was chosen to be the Pratt and Whitney J-58D used on the Lockheed SR-71 Blackbird. The SR-71 is still the world's fastest manned air-breathing aircraft. The airplane was designed to serve as a long-range reconnaissance vehicle and could fly at speeds upward of Mach 3.2 with a ceiling of about 85,000 ft (Ref. 6). The SR-71 was powered by two Pratt and Whitney J-58D engines. Each engine was an axial flow turbojet using a nine-stage compressor, two-stage turbine with

Presented as Paper 2005-3284 at the AIAA/CIRA 13th International Space Planes and Hypersonics Systems and Technologies Conference, Capua, Italy, 16–20 May 2005; received 6 June 2005; revision received 17 December 2005; accepted for publication 23 December 2005.

*Graduate Research Assistant, Department of Aerospace Engineering; Jesse.Colville@Aerojet.com. Member AIAA.

†Faculty Research Scientist, Department of Aerospace Engineering; RStarkey@umd.edu. Senior Member AIAA.

‡Professor, Department of Aerospace Engineering; Lewis@eng.umd.edu. Fellow AIAA.

bypass and produced 34,000 lb of thrust with the afterburner. It was the first jet engine designed to operate over long periods of time using its afterburner. At high Mach numbers, the turbomachinery was heavily bypassed, thereby creating a quasi-ramjet mode. In this way, the J-58D was an early combined cycle. Interestingly, a study[7,8] was completed in the mid-1990s looking at the SR-71 as the first stage of a small payload launch vehicle.

The SR-71 engine inlet operated as a mixed internal/external compression system. An intensive review of the inlet operation is given in the Ref. 9. The external system utilized a translating conical spike that retracted $1\frac{5}{8}$ in. per 0.1 Mach number starting near Mach 1.6 and ending at Mach 3.2 with shock-on-lip condition. The internal system consisted of a series of reflected shock waves followed by a terminal shock that is created by a step, effectively tripping the flow; the inlet self-starts when the spike begins to translate. Originally controlled by the pilot, the inlet system was outfitted with a digital automated flight and inlet control system[10] (DAFICS) in the early 1980s to allow for faster response to unstart.

The purpose of the translation, along with a complex sequence of bleeds[11–13] and bypasses, is to control the amount of flow entering the engine and to hold the terminal shock downstream of the throat (when $M_\infty > 1.6$) to avoid unstart. At low Mach numbers, the forward air inlet bypass doors open to exhaust air that is not needed by the engine. As the spike translates, the forward bypass doors begin to close to position the shock downstream of the throat. Shock trap and centerbody bleeds, along with aft bypass doors, also aid in the process of keeping the terminal shock in the correct position and to mitigate the effects of shock-wave/boundary-layer interactions. The spike translation increases the captured stream tube area from 8.7 to 18.5 ft^2. In the event of unstart of one of the engines, the DAFICS would push both engine spikes forward and control the bleeds and bypasses such that normal operation and normal shock position could be reobtained within seconds.

II. Methodology

All of the inlets considered in this study consisted of a centerbody spike acting as the lower surface and a cowl acting as the upper boundary. The modifications discussed include variations to the original centerbody angle and shoulder, as well as the cowl leading edge. No deviations from the basic design characteristics of the SR-71 were examined, all inlets remained axisymmetric designs. The mechanical feasibility of the proposed changes is not addressed in this study; however, work has been completed[14] (including hardware fabrication) on similar concepts incorporating complex variable geometry.

A method of characteristics algorithm[15,16] was developed to perform full external and internal inviscid supersonic flow analysis on axisymmetric combined-cycle inlets. This approach was used because of the computational speed of the code as well as control of the output. For the majority of the solution, the code maintained two vectors of flowfield data in memory to maximize computational time. (Continuous output of the data to temporary files was used to store the information needed to create flowfield contours.) An initial line of data is created by calculating the supersonic flow over a cone (numerical integration of the Taylor–Maccoll[17] equation). For the majority of the solutions, the initial data line consisted of 402 points. The remainder of the flow is analyzed by calculating the reflected internal oblique shock waves until a point where the flow is tripped at the throat and a lambda shock structure is formed. All of the thermodynamic properties are nondimensionalized by the freestream conditions.

The lambda shock system comprises three assumptions. The first is that a perfect 90-deg normal shock is propagated from the trip point and intersected with the last reflected oblique shock wave. At the intersection (or triple point), a slip line is formed. Across a slip line, flow angle and pressure must equal. However, meeting both of these criteria is impossible without a higher-order solution. Therefore, it was chosen to match flow angle instead of pressure. The third assumption is that a constant angle strong oblique shock wave is propagated from the triple point to the lower surface. The flow downstream of the throat is not considered here.

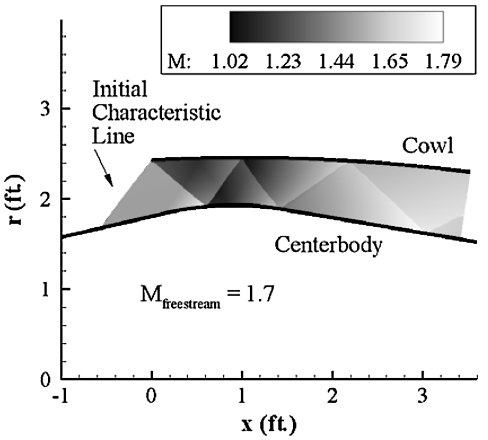

Fig. 1 Example output from axisymmetric method of characteristics algorithm (Mach number contours inside of a duct at freestream Mach Number of 1.7).

Other assumptions included a constant ratio of specific heats, γ, and level, steady flight at zero angle of attack. Although the constant gamma approach is suspect at hypersonic speeds, the assumption was deemed appropriate for this first-order study. An example contour plot of Mach number is shown in Fig. 1. Note the first zone of the contour plot represents the first-captured, left-running characteristic (the initial data line), not a shock wave. The reflected shock system is apparent as well as the prescribed lambda shock system at the exit. The upper and lower bounds of the duct are represented by the cowl and centerbody, respectively.

The main issues that are dealt with in the present work are total pressure recovery, flow distortion, and inlet starting. Total pressure recovery is important because it plays a key role in engine thrust and efficiency; the lower the recovery, the lower the thrust. In theory, the pressure losses can be augmented with an increase in fuel flow rate, but this leads to larger tank sizes and larger vehicle sizes (and lower specific impulse).

A flow is said to be distorted if the profiles of velocity, mass flux, and thermodynamic properties vary when looking at a cross-sectional piece of the flowfield. Compressors and combustors favor uniform flow properties; highly nonuniform flowfields can lead poor performance of these components. For the purpose this study, the distortion (or nonuniformity) is quantified as the difference between the minimum and maximum property, for example, χ, value divided by the area-averaged value at a cross section (from Seddon and Goldsmith[2]), or

$$(\chi_{\max} - \chi_{\min})/\chi_{\text{av}} = \Delta\chi/\chi_{\text{av}} \tag{1}$$

Area averaging was chosen to capture the spatial distribution of the flowfield properties. The flow properties before (supersonic) and after (subsonic) the lambda shock system are area averaged to characterize the flow quality entering the engine

The issue of inlet starting is highly critical because inlets for TBCC engines must function properly during transition from one cycle mode to another. In an inlet that utilizes internal supersonic compression the flow typically passes through a converging–diverging section. For an inlet to be self-started, supersonic flow must exist at the minimum area (or throat) of the duct. In essence, the inlet remains self-started if flow disturbances (both external and internal) do not change the captured air characteristics and the inlet is able to maintain supersonic flow at the throat. These disturbances could be a sudden rise in back pressure downstream of the throat, freestream perturbations, or boundary-layer separation. Preliminary estimates of internal contraction ratios that will self-start can be obtained by calculating the Kantrowitz limit (see Ref. 18). This limit is determined by first assuming a normal shock wave at the beginning of the internal compression section. The internal area ratio that produces sonic flow at the throat is then found by assuming one-dimensional, isentropic flow through the duct. For a perfect gas, the limit can be

calculated as follows:

$$\left(\frac{A_2}{A_4}\right) = \frac{1}{M_2}\left[\frac{(\gamma+1)M_2^2}{(\gamma-1)M_2^2+2}\right]^{\gamma/(\gamma-1)} \cdot \left[\frac{\gamma+1}{2\gamma M_2^2-(\gamma-1)}\right]^{1/(\gamma-1)} \times \left\{\frac{1+[(\gamma-1)/2]M_2^2}{(\gamma+1)/2}\right\}^{(\gamma+1)/2(\gamma-1)} \quad (2)$$

Note that M_2 in the Eq. (2) is the mass-averaged (as defined in Reference 18) Mach number across the cowl face. The maximum isentropic contraction ratio can be calculated as follows:

$$(A_4/A_o) = M_o[(\gamma+1)/2]^{(\gamma+1)/2(\gamma-1)} \cdot \left\{1+[(\gamma-1)/2]M_o^2\right\}^{-(\gamma+1)/2(\gamma-1)} \quad (3)$$

Van Wie[19] discusses experimental data found from a wide variety of inlets and compares their self-starting characteristics to that predicted by the Kantrowitz limit. This work shows that, under some circumstances, the Kantrowitz limit can be exceeded with bleed holes and/or bypasses.

III. SR-71 Inlet Analysis

No comprehensive diagrams of the SR-71 inlet were identified, and so a representative geometry had to be inferred from various YF-12 reports[20,21] and Ref. 9. The resultant geometry is shown in Fig. 2. The assumed inlet consisted of a 13-deg conical spike and circular arc inner cowl with a leading edge angle of 3 deg. The shoulder of the inlet (the transition from the linear spike to the linear rear section of the centerbody) was approximated by a cubic spline. The solid line in Fig. 2 is the position of the spike in the most forward position, and the dashed line is the position of the spike in the most aft (at the cruise speed) position. (Note the step in Fig. 2 at about $x = 3.5$ is the location of the throat section where the method of characteristics algorithm assumed the start of a lambda shock structure.)

Also note that the properties of the SR-71 inlet (and the proposed modifications) were calculated under the assumption that the incoming air is uniform and traveling at the flight Mach number. In reality, the flow will be perturbed depending on the placement of the inlet on the aircraft. In the real case of the SR-71, the flow entering the inlet is disturbed by the conical shock coming of off of the nose (~18-deg cone) of the vehicle. Computational fluid dynamics (CFD) analysis[22] performed on the SR-71 showed that the nose shock fell outside of the inlet at the design speed of Mach 3.2. Johnson and Montoya[20] reported that on average the local Mach number at the spike tip of the YF-12 (from flight data) was never more than 3% less than the freestream Mach number. This perturbation is less than the theoretical Mach number behind a conical shock off of an 18-deg cone; however, the shockwave patterns presented in Ref. 21 show that the bow shock wave has weakened before it draws near to the inlet, most likely due to the expansion waves generated

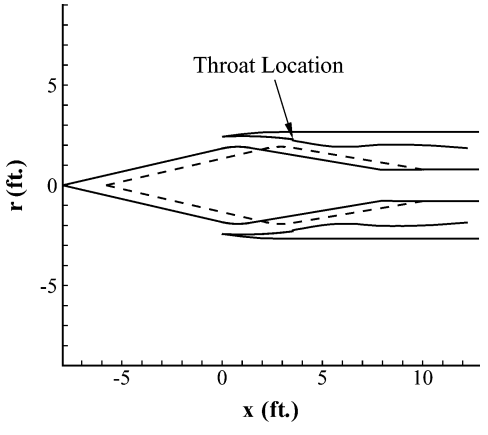

Fig. 2 Assumed inlet geometry.

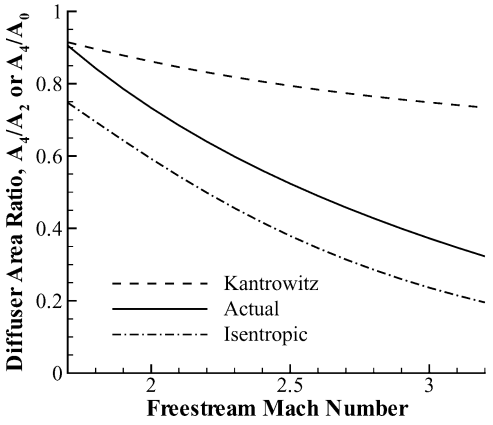

Fig. 3 SR-71 starting characteristics.

on the lateral surfaces of the vehicle. Nevertheless, as already stated, the effects of the nose shock are ignored in this analysis.

With use of the assumed area across the cowl face and at the throat, along with the mass-averaged Mach number entering the duct, the starting characteristics are calculated. Figure 3 is the resulting plot. Note Fig. 3, as well as Figs. 12, 14, 16, 18, and 20, plots the inverse of the Kantrowitz limit. As Fig. 3 shows, the inlet does indeed self-start at Mach 1.7, that is, the area ratio satisfy the Kantrowitz limit, and then proceeds to move away from the Kantrowitz limit, in parallel with the isentropic limit. Note that beyond Mach 1.7 the SR-71 inlet violates the Kantrowitz limit, but because the inlet incorporates variable geometry and flow control devices, it is able to remain started through Mach 3.2.

The flowfield properties of the SR-71 were then determined by applying the method of characteristics algorithm across the entire self-starting flight regime (Mach 1.7–3.2). Starting at Mach 1.7, the initial reflected shock off of the cowl leading edge intersects the centerbody on the shoulder, that is, the curved segment of the centerbody, causing the flow to reexpand to a higher than freestream Mach number (locally) (Note the reference contour in Fig. 1 shows contours of Mach number at a freestream speed of Mach 1.7.) This increase in local Mach number allows the second reflected shock to remain. This also produces a near-sonic (choked-flow) condition just downstream of the second reflection system. Because the shoulder continues to turn, the flow is able to expand, and subsequent shocks can be formed. The remainder of the shock train progresses, and the effect of the expansion waves propagating through the system is readily apparent. (The solutions shows about 6–7 total reflections.) Because of the presence of the expansion waves and shock train, temperature and pressure are near to or less than the freestream values at the throat entrance at the lower Mach numbers.

As the freestream Mach number increases and the spike retracts, the shock train progresses through the duct. The initial reflection off the cowl leading edge gradually moves off of the shoulder and onto the conical segment of the centerbody stopping any expansion before the first reflection. By Mach 2.5, the initial cowl shock has moved completely onto the conical section of the centerbody and the total number of reflections has been decreased to about 4. At Mach 3.2, only two or three reflections occur. Local regions of high temperature and pressure on the cowl are prevalent at Mach 3.2, but by the time the flow nears the throat, the temperature and pressure have decreased due to the presence of the expansion waves generated from the shoulder.

The area-averaged supersonic (entrance) and subsonic (exit) properties at the throat are shown in Figs. 4–8. The levels of distortion are quantified as well. The entrance pressure, temperature, and mass flow gradually rise with freestream Mach number. The supersonic throat Mach number initially decreases and then increases (with a final throat entrance Mach number of about 1.8), whereas the total pressure ratio initially increases and then decreases (while always remaining above 0.97) as the freestream speed is increased. The entrance total pressure ratio distortion is small and always stays below 3%. Distortion levels for Mach number and temperature are

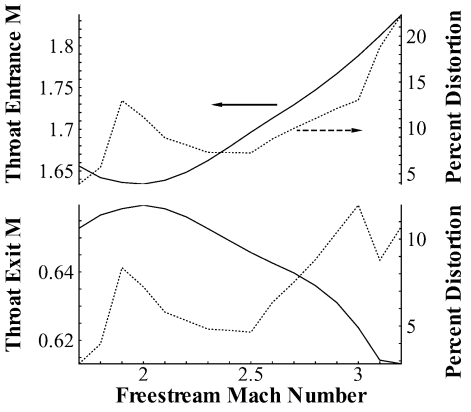

Fig. 4 Mach number at throat.

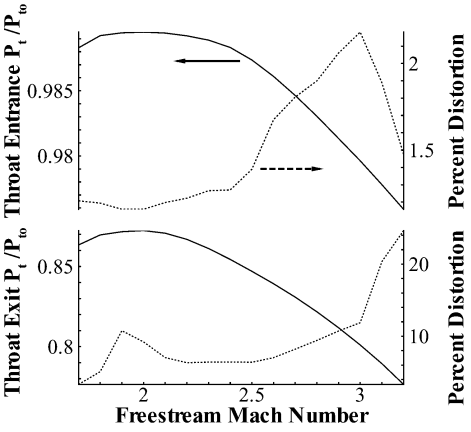

Fig. 5 Total pressure ratio at throat.

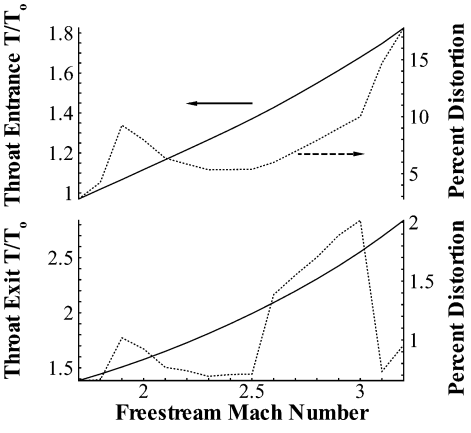

Fig. 6 Temperature ratio at throat.

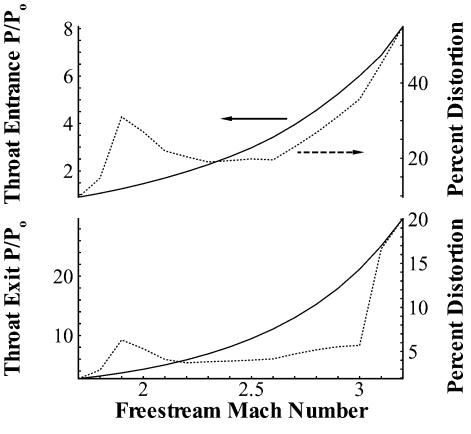

Fig. 7 Pressure ratio at throat.

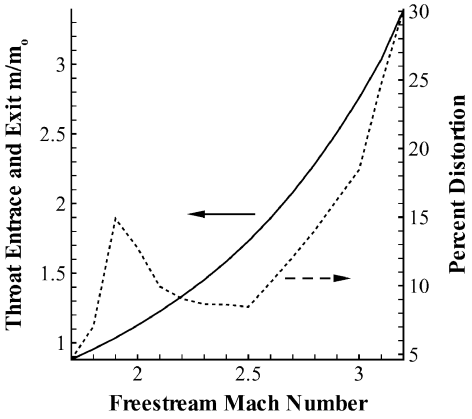

Fig. 8 Mass flow ratio at throat.

moderate, remaining at or below 20%. Pressure and mass flow distortion levels are large, rising to about 50 and 30%, respectively.

The subsonic exit conditions show that Mach number initially increases and then decreases (with a final throat exit Mach number of about 0.61), whereas all of the other flow properties have the same general trend as the supersonic entrance conditions. However, the levels of the distortion of the total pressure ratio increased significantly, whereas the levels of distortion of Mach number, temperature, and pressure decreased from the supersonic case. Any errors in the subsonic properties are a direct result of the assumed lambda shock structure.

As shown, the area-averaged temperature and pressure ratios exiting the inlet system at Mach 3.2 are about 2.8 and 30, respectively. In comparison to analysis performed on the actual SR-71 inlet, the pressure ratio found in this study is lower than the value of 40 reported by Kelly Johnson (former head of the Skunk Works) (see Ref. 23). The temperature ratio is below the maximum compressor inlet temperature ratio of 3.23 (assuming flight at 90,000 ft) (Ref. 11); however, real-gas and viscous effects have been ignored. The discrepancy between the quoted value and the result from this study can be accounted for by considering the changes to the flowfield as the air is directed through the subsonic portion of the original inlet before entering the compressor. If the flow (at a static pressure ratio of 30) were isentropically compressed to zero velocity, the pressure ratio would rise to 39, much closer to the quoted value.

IV. CFD Validation

CFD analysis was implemented to validate the method of characteristics (MOC) model. The program used in the validation process is NASA's OVERFLOW2,[24] a full Navier–Stokes solver. The accompanying grid generator is called OVERGRID.[25] Its many features include a hyperbolic grid generator and the ability to create separate, overlapping grids.

The grid used in the validation consisted of 701 points in the x direction and 101 points in the z direction. The grid is stretched at both ends of vertical plane and at the spike tip and cowl leading edge to improve the resolution of the shock waves. The solution used central differencing (fourth order) and the ARC3D three-factor diagonal scheme. The time step for iteration, or Courant–Freidricks–Lewy number, was determined locally. The ratio of specific heats was also held constant at 1.4.

A comparison of the Mach 3.2 freestream inviscid CFD results with the MOC results is shown in Figs. 9–11. The two solution methods agree quite well. The trends in the surface plots (Figs. 9–11) are nearly identical to that of the MOC. The only observable difference between the two sets of results is that the minimum Mach number predicted by the MOC solution is 0.6% higher than that of the CFD, as well a slight overprediction (0.01%) in the maximum temperature rise and a minor underprediction (0.4%) of the maximum pressure rise. The shock locations are accurately predicted by the MOC code (shown by the discontinuities). The run times for most cases of the MOC code (depending on the number of shock reflections) was on

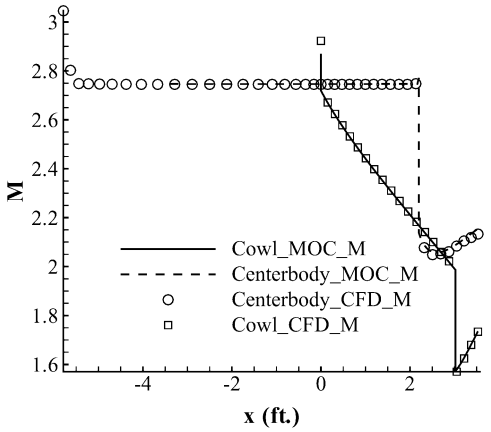

Fig. 9 Surface Mach number comparison.

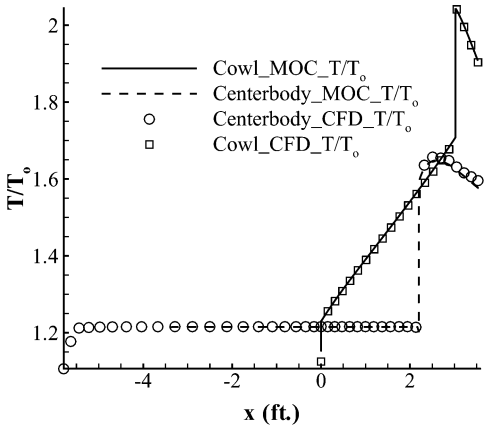

Fig. 10 Surface temperature ratio comparison.

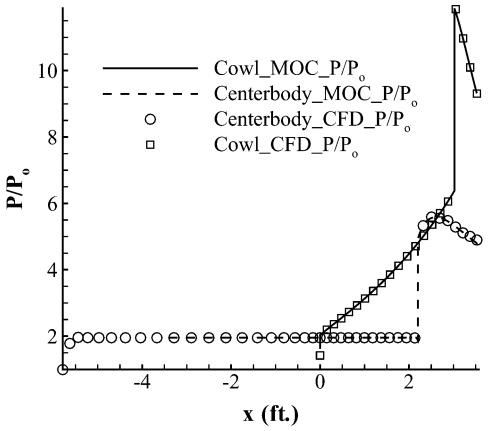

Fig. 11 Surface pressure ratio comparison.

the order of 15–20 s (with a grid four times as fine), whereas the CFD (at 500 iterations) results presented took a little over 3 min when run on a Dell Latitude D600 with a 1.6-GHz Pentium M processor and 1 GB of RAM. Additionally, a grid-reduction study was performed on the MOC code by reducing the initial characteristic data line to 51 points, while incorporating cubic spline interpolation and eliminating output of the flowfield contours; this reduced run times for a typical case to less than $\frac{1}{2}$ s.

V. Extending the Inlet Mach Number

To take full advantage of the capabilities of a TBCC engine, an appropriate inlet must be able to operate well above the maximum freestream Mach number of the SR-71 inlet. With no modification to the inlet, the centerbody spike shock will move inside of the

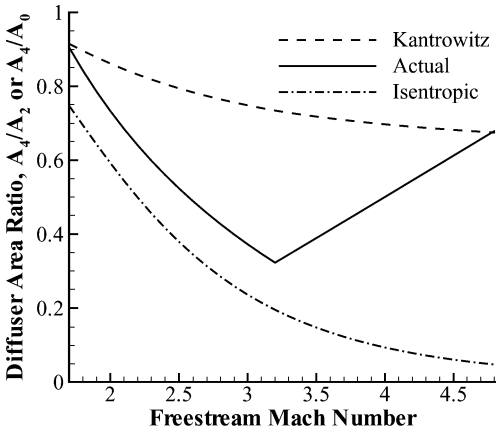

Fig. 12 Starting characteristics of the reextended spike.

cowl (past Mach 3.2) and the resulting inlet flowfield would likely degrade. A variety of means to achieve the overspeeding of the SR-71 inlet have been considered. Note that this is essentially a thought experiment because the J-58D itself could not operate into the Mach 6–7 regime. The effect on the overall system (especially mass and installation factors) due to the design changes will not be taken into account at this time. The constraints on these changes are that the slope of the duct after the throat remains fixed and the new designs will have to fit within the original SR-71 cowl.

A. Reextended Spike

The most obvious way to overspeed the inlet would be to reextend the centerbody spike in increments to maintain the shock-on-lip condition at the higher Mach numbers. When it is assumed that the spike could be extended to its original location at low speed, the inlet could be oversped up to a freestream Mach number of about 6.1. Beyond this point, the conical shock wave generated off of the spike would move inside of the cowl. Figure 12 shows the starting characteristics of this new operation. As shown in Fig. 12, the inlet would satisfy the Kantrowitz limit near a freestream Mach number of 4.8.

The flowfield properties show that, as freestream Mach number increases, the impingement location of the first reflected cowl shock advances onto and around the shoulder. This effect causes expansion waves to be generated before the first reflection off of the centerbody. As the spike advances and the initial reflection moves up and around the centerbody shoulder, local regions of high temperature and pressure are present along the cowl; however, these effects are eventually overcome by the presence of the expansion waves. The expanding of the duct also restricts the number of reflections: At Mach 4.0, two total reflections exist before the throat section. Large gradients in the flow properties are prevalent because of the considerable curvature of the leading-edge shock.

B. Variable Cowl Leading Edge

The second proposed redesign scheme involves allowing the radial portion of the cowl leading edge to vary while keeping the spike in its aft most position. This would enable the leading edge of the cowl to be aligned with the conical shock (as shown in Fig. 13) at every oversped Mach number. The dashed lines shown (starting from top to bottom) illustrate the cowl position at Mach numbers of 3.3, 3.6, 3.9, and 4.2, respectively. The resulting starting characteristics are shown in Fig. 14. As Fig. 14 shows, the inlet would satisfy the Kantrowitz limit near a freestream Mach number of 4.1. However, because of the rapid decrease in the cowl area, the diffuser area ratio would exceed 1.0 near Mach 4.7. This design would also introduce a large penalty in added cowl drag. Because of the limited operating range, full flow analysis of this redesign scheme was not completed.

C. Widened Shoulder Centerbody

The major problem with both of the preceding redesign schemes is the high rate at which the cowl/throat area ratio increases as the

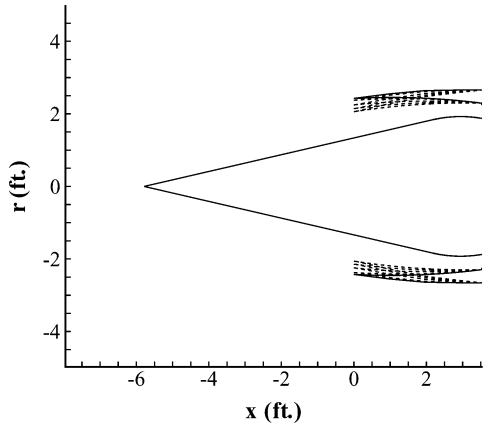

Fig. 13 Variable cowl leading-edge geometry.

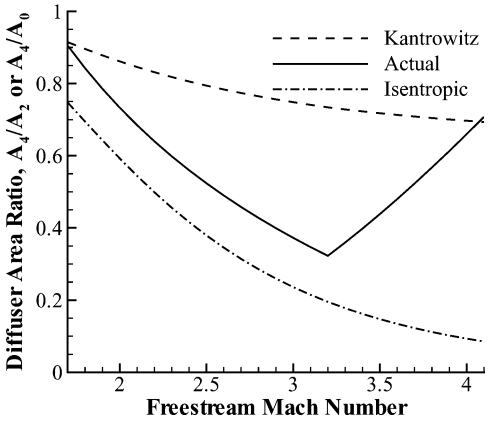

Fig. 14 Starting characteristics of the variable cowl leading-edge inlet.

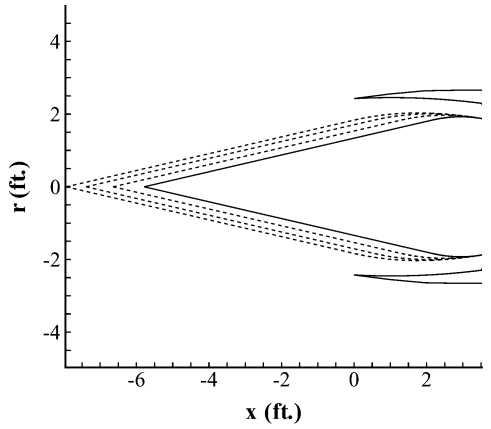

Fig. 15 Widened shoulder centerbody geometry.

inlet is oversped. One way to alleviate this problem is to fix the throat area while reextending the centerbody. To perform this operation, the shoulder on the centerbody spike would need to have the ability to widen as shown in Fig. 15. The dashed lines (going from right to left) in Fig. 15 represent the centerbody geometry at Mach numbers of 4, 5, and 6.1, respectively. The starting characteristics of the widened shoulder centerbody are shown in Fig. 16. Figure 16 shows that the inlet diffuser area ratio would violate the Kantrowitz limit up through Mach 6.1. However, assuming the inlet incorporates similar flow control devices that were used on the SR-71 inlet, it should be able to operate within the oversped flight regime. The inlet is mechanically limited by the reextension constraint imposed on the problem. If the inlet were allowed to reextend beyond the original low-speed location of the SR-71 inlet, it would likely be able to remain started past Mach 6.1.

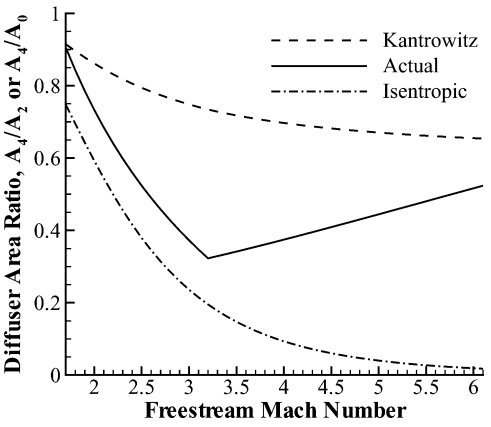

Fig. 16 Starting characteristics of the widened shoulder centerbody inlet.

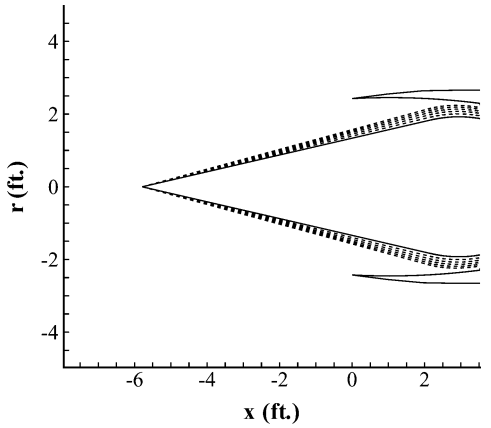

Fig. 17 Variable cone geometry.

The general trends of the flowfield properties are similar to that of the reextended spike except that the widened shoulder slows the progression of the initial reflected cowl shock onto the shoulder. Unlike the reextended spike, the reflected shock never moves completely over the shoulder. However, both systems result in only a two shock internal reflection system. Local regions of high temperature and pressure (where the temperature and pressure ratios rise to 2.4 and 15.24, respectively) are again apparent on the cowl before being affected by the expansion waves. Because the initial reflected cowl shock is not as curved for the widened shoulder centerbody, the gradients in the flow properties are not as severe as they are with the simple reextended spike.

D. Variable Cone Centerbody

Yet another option would be to install a variable angle cone on the centerbody spike. In this scenario, the spike would remain fixed in its axial location at Mach 3.2 and then increase its conical half-angle to maintain the shock-on-lip condition. However, this design has major limitations (beyond the obvious mechanical complexity) as shown in Fig. 17. The dashed lines in Fig. 17 are the change in the centerbody geometry needed to maintain the shock-on-lip condition at freestream Mach numbers of 3.3, 3.4, 3.5, 3.6, and 3.7. As Fig. 17 shows, the variable cone centerbody can only be enlarged up to an angle of about 15 deg (corresponding to a freestream Mach number of 3.7) before the throat would be completely closed. (Note that this design still assumes a cubic spline shoulder.) Besides the obvious physical problems with this inlet modification, Fig. 18 shows that the starting characteristics of this inlet are very poor. The inlet would violate the maximum isentropic contraction ratio limit (due to the decrease in throat area) before it penetrates the outer cowl. As with the variable cowl leading-edge design, this inlet was not fully analyzed due to its poor starting performance.

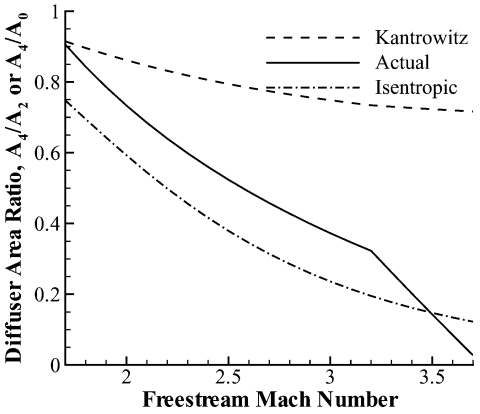

Fig. 18 Starting characteristics of the variable cone inlet.

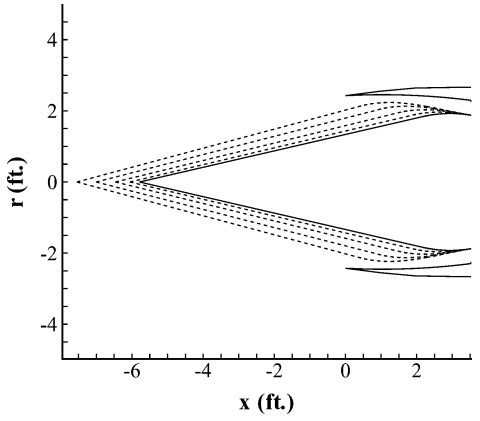

Fig. 19 Variable cone with reextension geometry.

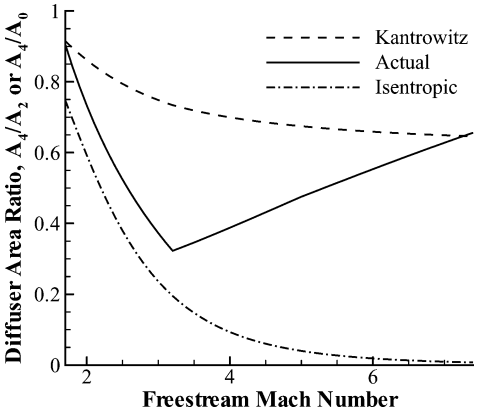

Fig. 20 Starting characteristics of the variable cone with reextension inlet.

E. Variable Cone with Reextension

The inlet shown in Fig. 19 can be constructed by combining the variable cone and reextension aspects. In this situation, as the spike is pushed forward the cone expands to maintain the shock-on-lip requirement. In the current design, the throat area remained fixed as well. Theoretically, this inlet could maintain the shock-on-lip condition for any freestream Mach number (where the maximum cone angle needed would only be about 16 deg) before reaching the reextension limit. The dashed lines correspond to the centerbody geometry (starting from right to left) at Mach numbers of about 3.5, 4, 5.25, and 8.25, respectively. Figure 20 shows that the variable cone with reextension inlet would satisfy the Kantrowitz limit at Mach 7.2.

The basic structures of the flowfield are very similar to that of the widened shoulder and the reextended spike schemes. However, the advancement of the impingement location of initial reflected cowl shock is slower than that of the widened shoulder, thus delaying the prereflection expansion. Accordingly, the impingement locations of the both the initial cowl reflected shock and the centerbody reflection appear to be constant from about Mach 5.5–7.2. The temperature and pressure ratio flowfields show a rather complex flow structure as the expansion waves propagate through the system, creating multiple regions of high and low temperature and pressure. The major difference between this scheme and the two earlier analyzed is that this design maintains the three reflected shock system through Mach 7.2.

F. Throat Property Comparisons

Gas properties at the throat for the three considered redesign schemes are shown in Figs. 21–25. The properties of the reextended spike inlet are shown by the dash–dotted lines, the widened shoulder centerbody by the dashed lines, and the variable cone with reextension the solid lines. Because of the limited number of shock reflections, the effective entry Mach number of the reextended spike remains one less than the flight Mach number for the entire flight regime. Entry total pressure losses are small mostly because of the small number of shock reflections. (The total pressure ratio remains above 0.86 at Mach 4.8.) Entry temperature, pressure, and mass flow ratios decrease to about 1.6, 4, and 2.3, respectively, as the inlet is oversped. However, all flow properties appear to be highly distorted. (The pressure and mass flow distortion levels are at 130 and 75%, at Mach 4.8, respectively.) This is expected because of the large curvature in the first reflected shockwave.

The Mach number at the throat exit of the reextended spike is rather low, beginning below Mach 0.6 and ending at about 0.45 (which is good for ramjet operation), but because the entry Mach numbers are high, the total pressure losses are substantial. (The total pressure ratio is about 0.7 at Mach 3.3 and falls to about 0.2 at Mach 4.8.) Exit pressure and temperature ratios are also large because of the high entry Mach numbers. (The temperature and pressure ratios are about 5.7 and 55 at Mach 4.8, respectively.) The distortion levels for Mach number and temperature ratio are acceptable (remaining below 10% for the entire regime), but the levels of distortion for total pressure, static pressure, and mass flow ratio are all still very high (above 50% for most of the regime) at the higher speeds.

The throat entrance and exit properties of the widened shoulder centerbody show a marked improvement in the flow quality over the reextended spike. At similar speeds, when compared to the reextended spike, the Mach number entering the throat is lower, the temperature and pressure are higher, and the distortion levels are much lower for four of the flow properties. The total pressure ratio is about the same entering the throat at similar speeds. The mass flow ratio similarly decreases from 3.37 at Mach 3.3 to 3.32 at Mach 6.1, but the change is sufficiently small such that the mass flow ratio is essentially constant. Figure 23 shows that the temperature ratio starts at about 1.8, decreases to about 1.75 near Mach 4, and then increases with a final ratio of about 2 at Mach 6.1. Similarly, the pressure ratio starts at about 7.7, then decreases to about 6.7 near Mach 4.5, and then increases with a final ratio of about 7 near Mach 6.1.

The exit properties of the widened shoulder centerbody also show that performance is better overall compared to the reextended spike. Total pressure ratio (starting at about 0.75 and ending below 0.2), Mach number (starting at about 0.59 and ending near 0.43), and pressure ratio (starting at 30 and ending at about 140), for any given Mach number, are higher than the reextended spike with slightly lower distortion levels. The temperature ratio (starting at about 3 and ending at about 8), interestingly, is essentially equal to the reextended spike, albeit with differing levels of distortion. In all likelihood, transition to scramjet would occur somewhere along the flight path because of the large increases in pressure ratio and the considerable losses in total pressure as the flight speed is increased.

The throat entrance and exit conditions of the variable cone with reextension design are comparable to the widened shoulder centerbody. At similar flight speeds, the entrance Mach number for the variable cone with reextension scheme is essentially the same as that of the widened shoulder. Likewise, the temperature and pressure

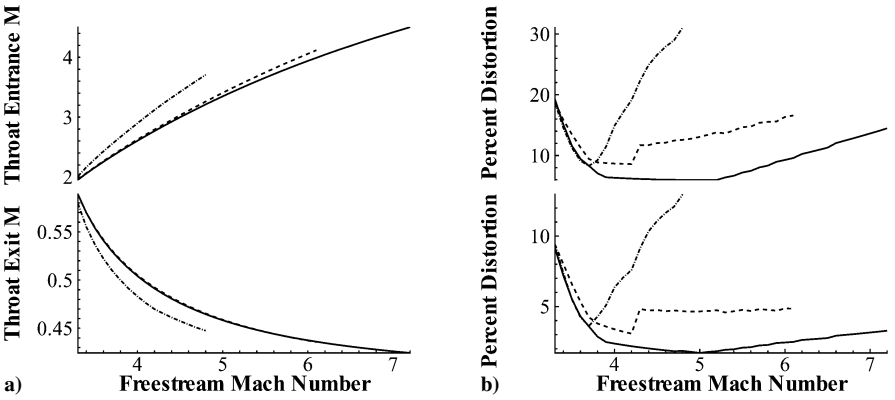

Fig. 21 Area-averaged throat Mach number comparisons: a) comparison of throat Mach numbers and b) distortion percentages: –·–·, reextended spike; – – –, widened shoulder centerbody; and ——, variable cone with reextension.

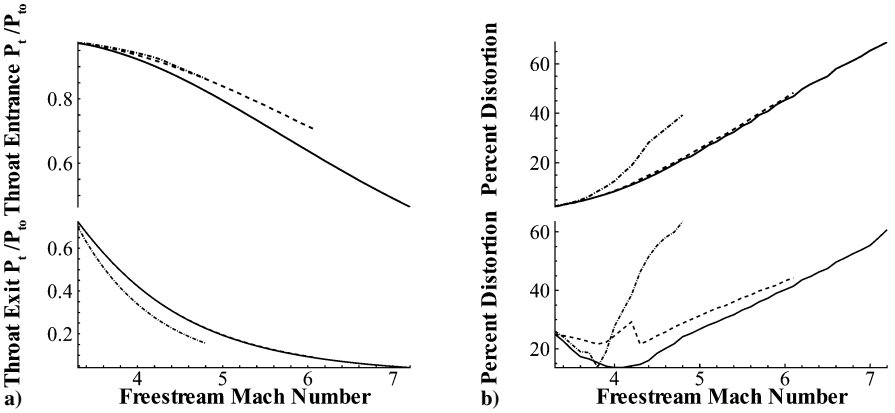

Fig. 22 Area-averaged throat total pressure ratio comparisons: a) comparison of throat total pressure ratios and b) distortion percentages: –·–·, reextended spike; – – –, widened shoulder centerbody; and ——, variable cone with reextension.

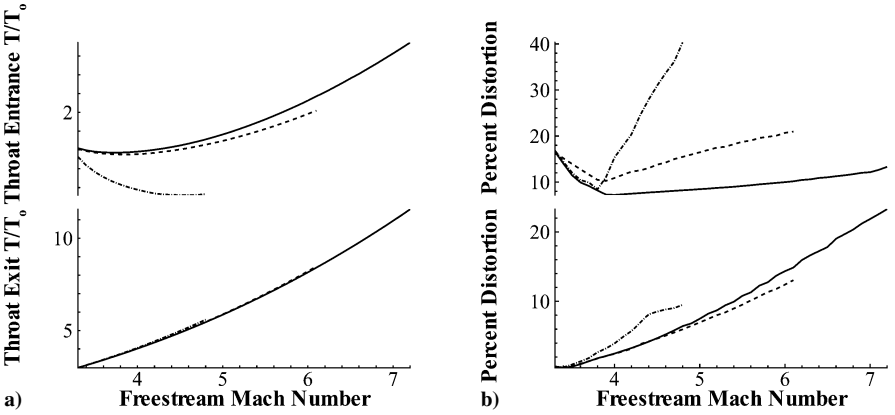

Fig. 23 Area-averaged throat temperature ratio comparisons: a) comparison of throat temperature ratios and b) distortion percentages: –·–·, reextended spike; – – –, widened shoulder centerbody; and ——, variable cone with reextension.

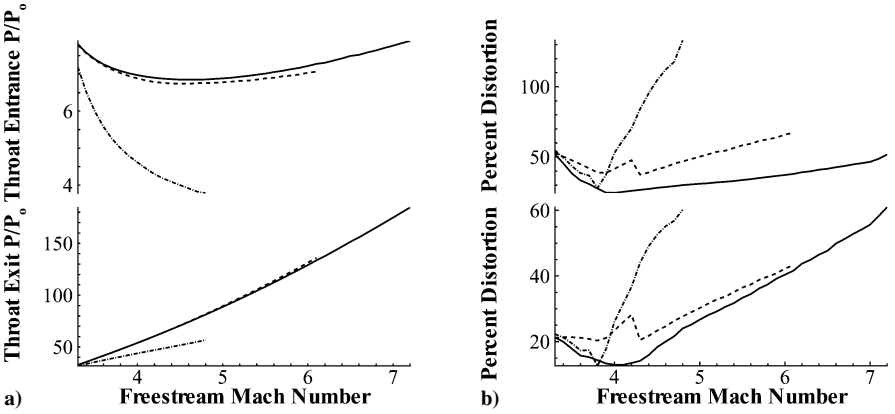

Fig. 24 Area-averaged throat pressure ratio comparisons: a) comparison of throat pressure ratios and b) distortion percentages: –·–·, reextended spike; – – –, widened shoulder centerbody; and ——, variable cone with reextension.

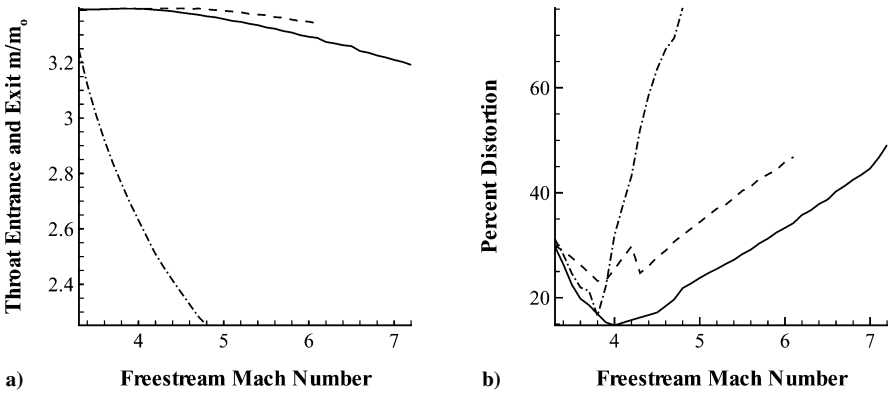

Fig. 25 Area-averaged throat mass flow ratio comparisons: a) comparison of throat mass flow ratios and b) distortion percentages: –·–·, reextended spike; – – –, widened shoulder centerbody; and ——, variable cone with reextension.

ratio entrance properties are similar, but the total pressure ratio is lower. This makes sense because in this case the flow passes through two stronger shock waves and an additional reflected shock. Overall, the distortion levels are slightly lower compared to the widened shoulder centerbody. Mass flow ratio decreases as well from 3.39 at Mach 3.3 to about 3.2 at Mach 7.2, but as with the widened shoulder, is essentially constant.

The exit properties of the variable cone with reextension inlet also show equivalent trends with the widened shoulder centerbody. The exit Mach number starts at about Mach 0.6 and finishes at about Mach 0.43. The total pressure ratio is effectively the same, starting at about 0.7 and ending below 0.1. The exit temperature and pressure ratios are fairly consistent; however, the distortion levels are moderately better for the variable cone with reextension inlet.

VI. Summary

This study developed a new strategy for designing inlets for TBCC engines. Rather than starting the design process with a clean slate, the performance of a specific supersonic inlet was analyzed and certain aspects of the inlet were redesigned to see if the flight envelope could be pushed into the hypersonic regime. A computationally fast numerical model was developed using the axisymmetric MOC that is capable of calculating the supersonic, inviscid flow properties of axisymmetric inlets. This results from the model were used to quantify important properties of the flowfield (Mach number, total pressure ratio, temperature ratio, pressure ratio, and mass flow ratio) and their levels of distortion (spatial nonuniformity) at the throat. A simple lambda shock structure was then used to approximate the flow properties leaving the throat. The Kantrowitz limit was computed to estimate the starting limits of the inlets.

In this work, a TBCC-like engine after the J-58D engines used on the Lockheed SR-71 was chosen as baseline. The engines effectively operated as a ramjet at the higher speeds because a good deal of the airflow bypassed the combustor and turbine and was dumped straight into the afterburner. Accordingly, the SR-71 inlet was modeled as a low-speed TBCC inlet. The inlet of the SR-71 is a mixed compression inlet that starts at Mach 1.7 and can be accelerated up to Mach 3.2. The inlet utilizes a translating spike and a series of bleeds and bypasses to control the position of the terminating normal shock and to regulate the amount of airflow passing through the engine.

Investigation of the SR-71 inlet proved that the inlet indeed satisfies the Kantrowitz limit at Mach 1.7 and maintains the starting capability through Mach 3.2. The characteristics model showed that at the low Mach numbers several reflected shock waves are present within the duct. As the inlet speeds up, the shock train propagates through the duct so that at the design Mach number of 3.2 only two internal reflections are present. The inlet performed rather well, losing less than 3% of total pressure (with very low levels of distortion) before entering the throat. Downstream of the throat, the total pressure losses stayed above about 23% and the Mach number remained nearly constant, varying from 0.66 to 0.62 at flight speeds between Mach 1.7 and 3.2. Pressure, temperature, and mass flow ratios gradually rose at the exit plane as the Mach number was increased. The Mach 3.2 inviscid solution was validated using NASA's OVERFLOW2 CFD tool.

Five modifications to the inlet were then proposed, and their high-speed performance (>Mach 3.2) was evaluated. Two schemes, the variable cowl leading edge and the variable cone centerbody, performed poorly: both exhibited substandard starting characteristics. The simplest (and least expensive) redesign method, the reextended spike, demonstrated the ability to satisfy the Kantrowitz limit at and beyond Mach 4.8. However, the flowfield properties were highly distorted because the initial reflected cowl shock moved all of the way around the shoulder of the centerbody, causing rather significant gradients in the flow.

The remaining two schemes, the widened shoulder centerbody and the variable cone with reextension, showed some promise. The widened shoulder centerbody inlet violated the Kantrowitz limit through Mach 6.1, whereas the variable cone with reextension inlet would not satisfy the Kantrowitz limit until Mach 7.1. However, both inlets should be able to remain started with the use of similar flow control devices that were used on the SR-71 inlet. Both inlets displayed comparable flowfield properties at the exit plane. The Mach number entering the throat started around Mach 2.0 and increased at the same rate for both inlets. Similarly, for both inlets the temperature ratio entering the throat started at about 1.8, decreased, and then increased at about the same rate. Likewise, the pressure ratio entering the throat started at about 7.7, decreased, and then increased at similar rates. The main difference in the throat entrance properties between the two schemes is that the total pressure ratio is consistently higher for the widened shoulder centerbody and that the distortion levels for the variable cone with reextension scheme are steadily lower. The mass flow at the throat was also slightly higher for the widened shoulder centerbody. The area-averaged subsonic flow properties are fundamentally the same for both schemes. Both of these inlets exhibited very large levels of static temperature and pressure at the throat exit at higher speeds suggesting that transition to scramjet operation could be possible.

The overriding conclusion of this study is that complex variable geometry is probably needed to design an inlet that is operable over a span of flight speeds that ranges from the low supersonic regime into the hypersonic corridor. The mechanical complexity associated with the complex variable geometry is the main obstacle that would need to be overcome to realize either of the two promising redesign schemes developed in this work. This point underscores the difficulty in constructing a single common inlet that would properly feed the three cycles of a TBCC engine. More detailed flow analysis, including viscous and boundary-layer control, is needed to quantify the flowfield properties and self-starting characteristics of both concepts better. Finally, coupling this numerical tool to gas turbine, ramjet, and scramjet models is essential.

Acknowledgments

This work has been sponsored by the Space Vehicle Technology Institute, under Grant NCC3-989, one of the NASA University Institutes, with joint sponsorship from the Department of Defense. Appreciation is expressed to Claudia Meyer of the NASA John H. Glenn Research Center and to John Schmisseur and Walter Jones of the U.S. Air Force Office of Scientific Research.

References

[1]Clough, J., "Modeling and Optimization of Turbine Based Combined Cycle Engine Performance," M. S. Thesis, Dept. of Aerospace Engineering, Univ. of Maryland, College Park, MD, Dec. 2004.

[2]Seddon, J. J., and Goldsmith, E. L., *Intake Aerodynamics*, 2nd ed., AIAA Education Series, AIAA, Reston, VA, 1999.

[3]Seddon, J. J., and Goldsmith, E. L. (eds.), *Practical Intake Aerodynamic Design*, AIAA Education Series, AIAA, Washington, DC, 1993.

[4]Mahoney, J. J., *Inlets for Supersonic Missiles*, AIAA Education Series, AIAA, Washington, DC, 1990.

[5]Fernandez, R., Reddy, D. R., Benson, T. J., Iek, C., Biesiadny, T. J., and Wendt, B. J., "Design Issues for Turbine-Based and Rocket-Based Combined Cycle Propulsion System Inlets," AIAA Paper 98-3774, July 1998.

[6]*SR-71 Online Aircraft Museum*, http://www.sr-71.org [cited 31 June 2003].

[7]Anderson, E. C., and Lopata, J. B., "Using a Modified SR-71 Aircraft and Air-Launched Expendable Rockets to Place Small Payloads into Orbit," AIAA Paper 96-2774, July 1996.

[8]Anderson, E. C., Lopata, J. B., Hoar, P. R., Nelson, D., "Performance Analysis and Optimized Design of an SR-71 Based Air Launch System for Small Payloads," AIAA Paper 97-36557, July 1997.

[9]*SR-71 Flight Manual*, http://www.sr-71.org/blackbird/manual/index.htm [cited 3 July 2003].

[10]Reukauf, P. J., Burcham, F. W., and Holzman, J. K., "Status of a Digital Integrated Propulsion/Flight Control System for the YF-12 Airplane," AIAA Paper 75-1180, Sept. 1975.

[11]Syberg, J., and Hickcox, T. E., "Design of a Bleed System for a Mach 3.5 Inlet," NASA CR-2187, Jan. 1973.

[12]Cole, G. L., Dustin, M. O., and Nienер, G. H., "A Throat-Bypass Stability System for a YF-12 Aircraft Research Using Self-Acting Mechanical Valves," NASA TM-X-71779, Sept. 1975.

[13]Cole, G. L., Dustin, M. O., and Niener, G. H., "Continuous-Output Terminal-Shock-Position Sensor for Mixed Compression Inlets Evaluated in Wind Tunnel Tests of YF-12 Aircraft Inlet," NASA TM-X-3144, Dec. 1974.

[14]Saunders, J. D., and Linne, A. A., "Status of the Variable Diameter Centerbody Inlet Program," *NASA Langley Research Center, First Annual High-Speed Research Workshop*, Pt 3, 1992, pp. 1483–1504.

[15]Ferri, A., "The Method of Characteristics," *High Speed Aerodynamics and Jet Propulsion. Vol. VI. General Theory of High Speed Aerodynamics,* edited by W. R. Sears, Princeton Univ. Press, Princeton, NJ, 1954, Sec. G., pp. 583–668.

[16]Ferri, A., "Application of the Method of Characteristics to Supersonic Rotational Flow," NACA TR-841, April 1946.

[17]Taylor, G. I., and Maccoll, J. W., "The Air Pressure on a Cone Moving at High Speed," *Proceedings of the Royal Society of London*, Vol. 139, 1933, pp. 278–311.

[18]Kantrowtz, A., and Donaldson, C., "Preliminary Investigation of Supersonic Diffusers," NACA Rept. ACR L5D20, May 1945.

[19]Van Wie, D. M., "Scramjet Inlets," *Scramjet Propulsion*, edited by E. T. Curran and S. N. B. Murthy, Progress in Astronautics and Aeronautics, Vol. 189, AIAA, Reston, VA, 2000, Chap. 7, pp. 447–512.

[20]Johnson, H. J., and Montoya, E. J., "Local Flow Measurements at the Inlet Spike Tip of a Mach 3 Supersonic Cruise Airplane," NASA TN D-6987, May 1973.

[21]Cole, G. L., Cwynar, D. S., and Geyser, L. C., "Wind-Tunnel Evaluation of the Response of a YF-12 Aircraft Flight Inlet to Internal Airflow Perturbations by Frequency-Response Testing," NASA-TM-X-3141, Dec. 1974.

[22]Tomaro, R. F., and Wurtzler, K. E., "High Speed Configuration Aerodynamics: SR-71 to SMV," AIAA Paper 99-3204, July 1999.

[23]Miller, J., *Lockheed Martin's Skunk Works*, rev. ed., Midland Pub., Leicester, England, U.K. 1995.

[24]Buning, P. G., Jespersen, D. C., Pulliam, T. H., Chan, W. M., Slotnick, J. P., Krist, S. E., and Renze, K. J., "Overflow User's Manual," Ver. 1.8aa, NASA Langley Research Center, April 2003.

[25]Chan, W. M., Chiu, I.-T., and Buning, P. G., "User's Manual for the HYP-GEN Hyperbolic Grid Generator and the HGUI Graphical User Interface," NASA TM 108791, Oct. 1993.